Atmos. Chem. Phys. Discuss., 11, 14339–14381, 2011
www.atmos-chem-phys-discuss.net/11/14339/2011/
doi:10.5194/acpd-11-14339-2011

Atmospheric Chemistry and Physics Discussions

Impact of dust aerosols on Hurricane Helene's early development through the deliquescent heterogeneous freezing mode

H. Zhang, I. N. Sokolik, and J. A. Curry

School of Earth and Atmospheric Sciences, Georgia Institute of Technology, Atlanta, GA, USA

Received: 24 March 2011 – Accepted: 28 April 2011 – Published: 10 May 2011

Correspondence to: H. Zhang (henian.zhang@eas.gatech.edu)

Published by Copernicus Publications on behalf of the European Geosciences Union.

Abstract

An ice nucleation parameterization accounting for the deliquescent heterogeneous freezing (DHF) mode was implemented into the Weather Research Forecast (WRF) model. The DHF mode refers to the freezing process for internally mixed aerosols with soluble and insoluble species that can serve as both cloud condensation nuclei (CCN) and ice nuclei (IN), such as dust. A modified version of WRF was used to examine the effect of Saharan dust on the early development of Hurricane Helene (2006) via acting as CCN and IN. The WRF simulations showed the tendency of DHF mode to promote ice formation at lower altitudes in strong updraft cores, increase the local latent heat release, and produce more low clouds and less high clouds. The inclusion of dust acting as CCN and IN through the DHF mode modified the storm intensity, track, hydrometeor distribution, cloud top temperature (hence the storm radiative energy budget), and precipitation and latent heat distribution. However, changes in storm intensity, latent heating rate, and total precipitation exhibit nonlinear dependence on the dust concentration. Improvement in the representation of atmospheric aerosols and cloud microphysics has the potential to contribute to better prediction of tropical cyclone development.

1 Introduction

During summer and early fall, North Atlantic tropical cyclones (TCs) and their precursors are often observed to interact with a hot, dry, and dusty air mass originating from the Sahara Desert. This air mass is often referred to as the Saharan Air Layer (SAL) (Carlson and Prospero, 1972; Karyampudi et al., 1999; Dunion and Velden, 2004). The SAL is thought to affect the development of North Atlantic TCs from several aspects. From a dynamic and thermodynamic perspective, the SAL may affect the TC development in multiple ways (Karyampudi and Pierce, 2002; Dunion and Velden, 2004; Wu, 2007; Jones et al., 2007; Sun et al., 2008, 2009; Shu and Wu, 2009; Reale et al.,

ACPD
11, 14339–14381, 2011

2009; Braun, 2010). Dust embedded in the SAL can modify the atmospheric temperature stratification through interacting with solar and infrared (IR) radiation (Guedalia et al., 1984; Sokolik et al., 2001; Chen et al., 2010), and thus affect the TC development (Karyampudi and Carlson, 1988; Karyampudi and Pierce, 2002). Dust is also hypothesized to suppress Atlantic TC activity through reducing the sea surface temperature (SST) (Evan et al., 2006; Wu, 2007; Wong et al., 2008; Lau and Kim, 2007; Evan et al., 2009).

In addition to the radiative impacts, dust particles can act as cloud condensation nuclei (CCN), giant CCN (GCCN), and ice nuclei (IN), affecting the cloud droplet concentration and size, precipitation process, and lifetime of clouds (Levin et al., 1996; DeMott et al., 2003, 2009; Field et al., 2006; Ansmann et al., 2008; Connolly et al., 2009; Kumar et al., 2009a, 2009b; Pratt et al., 2009; Eidhammer et al., 2010; Wiacek et al., 2010). The impact of dust as nucleating aerosols on various cloud systems has been reported by many previous studies based on in situ and remote sensing observations and modeling. Rosenfeld et al. (2001) found that shallow cumulus clouds forming in dusty regions contained smaller cloud droplets and produced less precipitation. Mahowald and Kiehl (2003) found a positive relationship between the amount of thin low clouds and mineral aerosols over Africa and the North Atlantic. Increase in shallow cumulus cloud coverage has been found under dusty conditions over the Eastern Atlantic (Kaufman et al., 2005). During the NASA African Monsoon Multidisciplinary Activities (NAMMA) field campaign based in Cape Verde (Zipser et al., 2009), it was found that as much as 79 % of residual particles from liquid cloud droplets in selected clouds embedded in the SAL were composed of mineral dust (Twohy et al., 2009). The cloud droplet number concentration in dust-polluted clouds was higher than in clean marine clouds.

The ice nucleating ability of dust has been known for a long time (Isono et al., 1959). The nucleation ability of dust may vary strongly, depending on temperature and its mineralogical composition (Field et al., 2006). High correlation between the presence of dust and ice formation in altocumulus clouds over Asia has been reported by Sassen

ACPD
11, 14339–14381, 2011

(2002). High concentrations of IN with a maximum value greater than 0.3 cm^{-3} have been found in a long-lived SAL near Florida (DeMott et al., 2003, 2009) that might have caused a seeding effect on altocumulus cloud formed at the upper boundary of the SAL (Sassen et al., 2003). Evidence of high concentrations of cloud ice particles in deep convective clouds affected by Saharan dust has been reported at altitudes where heterogeneous ice nucleation prevails (Min et al., 2009; Li and Min, 2010), leading to higher cloud effective temperature (Min and Li, 2010).

Numerical models have also been used to study the effect of dust on cloud development. Levin et al. (2005) found that, without the effect of ice nucleation, dust as GCCN greatly enhanced the precipitation in continental clouds but not in maritime clouds. With dust as IN, precipitation in both types of clouds was reduced. Van den Heever et al. (2006) found that an increase in the aerosol concentration associated with a Saharan dust outbreak led to stronger and more frequent updrafts, which enhanced the production of supercooled liquid water at upper levels. Freezing of these supercooled cloud droplets into ice particles released a large amount of latent heat, which in turn supported intense updrafts. Yin and Chen (2007) suggested that the impact of dust on cloud development depends on the dust vertical distribution. When the majority of dust was below 3 km where temperature was greater than −5 °C, introducing more dust as CCN tended to suppress the precipitation. However, when dust was at temperatures less than −5 °C, dust acting as IN either enhanced or suppressed the precipitation, depending upon the concentration and several other factors. The overall impact of aerosols, including dust, on precipitation is thought to depend upon the cloud type and meteorological conditions (Khain et al., 2008).

Recently, there have been several studies specifically focusing on the impact of aerosols on TC development. Rosenfeld et al. (2007) reported that turning off the warm rain formation in numerical simulations of Hurricane Katrina altered the storm track and reduced the storm intensity, and hence proposed that seeding of small CCN could lead to weakening of storms. Khain et al. (2008) proposed that continental aerosols may contribute to the intense lightning occurrences and modify the development of

ACPD
11, 14339–14381, 2011

hurricanes that are close to the land. Khain et al. (2010) suggested that continental aerosols can invigorate convection at TC periphery and lead to weaker storms. Targeting at the effect of Saharan dust as nucleating aerosols on TC development, our previous studies (Zhang et al., 2007, 2009; Zhang 2008) suggested that dust in the eyewall development region can affect the eyewall evolution by changing the distribution of latent heat, and hence trigger changes in dynamic and thermodynamic processes that ultimately modify eyewall intensity. Once rainbands formed, large amounts of dust could not reach the eyewall. In this case dust acting as CCN can affect the eyewall indirectly by modulating rainband development, as intense convection in rainbands can adversely affect eyewall intensification by causing latent heat release away from the eyewall, enhancing cold pools and blocking the surface radial inflow. The major latent heating from cloud diffusional growth process and convection intensity in both eyewall and rainbands did not show monotonic relation with the input CCN concentration.

Recently, there has been considerable interest in nucleation ability of aerosols containing both soluble and insoluble part, such as dust particles (Petters and Kreidenweis, 2007; Diehl and Wurzler, 2004; Phillips et al., 2008; Kumar et al., 2009a, b; Khvorostyanov and Curry, 2000). In particular, Khvorostyanov and Curry (2000) proposed that a dust particle can act as CCN to form a cloud droplet first and then serve as IN to help cloud droplets freeze, which was referred to as the deliquescent heterogeneous freezing (DHF) mode. However, most mesoscale numerical models used for TC forecasting assume a clean environment and the microphysical parameterizations usually do not consider this mechanism. Here we examine the impact of dust aerosols on the early development of a real TC, Hurricane Helene (2006), by conducting WRF simulations with and without the ice nucleation parameterization accounting for the DHF mode. The goal of this study is to examine the extent to which dust aerosols can influence the intensity, track, and structure of a developing TC through the cloud microphysical processes. Remote sensing observations from Cloud-Aerosol Lidar and Infrared Pathfinder Satellite Observation (CALIPSO), CloudSat, Moderate Resolution Imaging Spectroradiometer (MODIS), and Tropical Rainfall Measuring Mission (TRMM)

ACPD
11, 14339–14381, 2011

were utilized to examine the distributions and characteristics of dust particles, hydrometeors, cloud top temperature, latent heat release and precipitation, as well as to constrain and evaluate the WRF model.

2 Development of the pre-Helene mesoscale convective vortex

On 11 September 2006, a massive mesoscale convective system (MCS) associated with a tropical easterly wave moved off the coast of Africa (Fig. 1a). The diameter of the MCS was more than 1000 km. By 12:00 UTC 12 September, the system was classified as a tropical depression with an estimated maximum sustained surface wind speed of 13 m s^{-1} and a minimum sea level pressure (MSLP) of 1007 hPa. The storm slowly strengthened and became Tropical Storm Helene on 00:00 UTC 14 September with maximum sustained winds of 18 m s^{-1}. While moving westward, Helene continued to develop and eventually became a category 3 hurricane at 06:00 UTC 18 September with estimated MSLP of 955 hPa and maximum sustained winds of 54 m s^{-1}.

Here, we focus on the period between 11–13 September during which an extended layer of Saharan dust was present to the north and northwest quadrant of the storm (Fig. 1). The horizontal and vertical distributions of dust were further examined using remote sensing observations from the NASA A-Train satellites including the Aqua and CALIPSO. The A-Train satellites cross the equator at around 01:30 p.m. local time, trailing each other by just a few minutes and providing near-simultaneous measurements of the atmosphere and surface. The MODIS instrument onboard Aqua measures radiances in 36 spectral bands ranging in wavelength between 0.4 to 14.4 µm. Data used in this study include the MODIS/Aqua Collection 5 Level 2 aerosol product (MYD04) and cloud product (MYD06), which have a horizontal resolution of 10 km. Figure 2a shows the aerosol optical depth (AOD) and cloud effective radius retrieved by MODIS between 13:55 UTC to 15:40 UTC on 12 September. A dust plume with AOD greater than 0.5 and a width more than 300 km can be seen immediately north of the storm. Clouds with small effective radii developed in the midst of dust. The Cloud-Aerosol Lidar with

ACPD
11, 14339–14381, 2011

Orthogonal Polarization (CALIOP) onboard CALIPSO crossed the dust plume between 15:38 and 15:44 UTC on 12 September. Figure 2b shows the dust layer extending from near surface to 5 km. The presence of abundant Saharan dust made Helene an ideal case to study the impact of dust on TCs.

During the NAMMA field campaign, the NASA DC-8 aircraft flew into the pre-Helene tropical depression on 12 September. On the northwest side of the circulation center adjacent to the dust layer, strong convection was observed with a maximum radar reflectivity more than 50 dBZ just above the melting level at 4 km (Zipser et al., 2009). Jenkins et al. (2008) and Jenkins and Pratt (2008) found that vertical velocities, cloud water content, ice concentrations, and lightning activities were very high. They hypothesized that dust invigorated convection in the region. The concentration of particles with diameters between 3–50 µm at the temperature level of −44 °C in the anvil clouds was as high as 300 cm^{-3} and residual particles from these ice crystals were mostly dust (Heymsfeld et al., 2009). The highest concentration was found in strong updrafts that developed from the boundary layer with high aerosol loading. Heymsfeld et al. (2009), therefore, suggested that ice crystals at temperature level of −44 °C were produced through homogeneous freezing of cloud droplets that formed on dust particles. Samples of anvil clouds from other parts of the storm were not collected during this particular flight. However, dust particles were found in the ice crystal residual samples from anvil clouds away from the dust source during a NAMMA flight into the pre-Gordon MCS (Cynthia Twohy, personal communication, 2010). This suggests that storm circulation may bring dust and hydrometeors containing dust to a much larger area.

3 Model configuration

To examine the sensitivity of the pre-Helene MCS to the dust particles through ice nucleation process, numerical experiments were conducted with the Weather Research and Forecast Model (WRF) version 3.1 developed at the National Center for

ACPD
11, 14339–14381, 2011

Atmospheric Research (NCAR). The WRF dynamics solves fully compressible, nonhydrostatic Euler equations formulated on the terrain-following hydrostatic-pressure vertical coordinate (denoted by η). Our simulations covered the three-day period from 00:00 UTC 11 September to 00:00 UTC 14 September during which the pre-Helene MCS moved off the African coast and gradually intensified into a tropical depression and then a tropical storm. Two nested domains with a horizontal resolution of 15 km and 5 km were used. The inner Domain 2 was initialized at 12:00 UTC 11 September, which was 12 h later than the outer Domain 1. The number of horizontal grid points for Domain 1 and Domain 2 were 357×212 and 634×412, respectively. There were 31 η layers in the vertical direction between the surface and 20 km a.s.l. The NCEP FNL (Final) Operational Global Analysis data on a 1° by 1° grid every 6 h were used as the initial and boundary conditions for Domain 1.

The Yonsei University planetary boundary layer (PBL) scheme was used in the simulations, which features an explicit treatment of entrainment at the top of PBL. The Noah Land Surface Model (LSM) was selected to provide the vertical transport of sensible and latent heat fluxes to the PBL scheme. The Goddard shortwave radiation scheme and the Rapid Radiative Transfer Model (RRTM) longwave radiation scheme were selected for radiative transfer computations. The Betts-Miller-Janjic cumulus convection scheme was used for Domain 1.

The Morrison double-moment cloud microphysics scheme (Morrison et al., 2005; Morrison and Pinto, 2005) was chosen. It is a two-moment scheme that predicts the mixing ratio and number concentration of five hydrometeors: cloud droplets, ice crystals, snow, rain, and graupel. The hydrometeor size distribution follows a generalized gamma distribution. The Morrison scheme is modified here by inclusion of a heterogeneous ice nucleation parameterization that accounts for dust's ability to serve as both CCN and IN, which will be discussed below.

ACPD
11, 14339–14381, 2011

3.1 Inclusion of an ice nucleation parameterization accounting for the DHF mode

In the Morrison scheme, all aerosols are currently assumed to be ammonium sulfate. The activated aerosol number is related to the aerosol size distribution, composition and supersaturation through a parameterization developed by Abdul-Razzak et al. (1998) and Abdul-Razzak and Ghan (2000), which is based on the Köhler theory (Köhler, 1936). In classical heterogeneous ice nucleation theory, IN can lead to the ice formation through condensation, immersion, contact and deposition freezing modes (Vali, 1985; Pruppacher and Klett, 1997). The heterogeneous ice nucleation parameterization in the Morrison scheme includes the contact freezing mode (Meyers et al., 1992), immersion freezing mode (Bigg, 1953), and deposition/condensation freezing mode (Cooper, 1986). The IN production is a function of temperature.

The current treatment of CCN and IN in the Morrison scheme does not adequately represent the scenario occurring in clouds formed in dusty conditions. Dust particles can act as both CCN and IN due to the fact that they contain both soluble and insoluble materials. To address this issue, a heterogeneous ice nucleation parameterization for internally mixed aerosols based on a series of papers published by Khvorostyanov and Curry was implemented into the Morrison microphysics scheme. Khvorostyanov and Curry (2000) proposed a new generalized theory of heterogeneous ice nucleation for internally mixed aerosols that depends on both temperature and supersaturation. This theory allows ice crystal formation via condensation freezing at subsaturation over water but supersaturation over ice, which can be used to explain the observed high nucleation rates at relatively warm temperatures (−5 to −12 °C). Khvorostyanov and Curry (2004, 2005) extended this theory and developed a framework suitable for cloud-scale and large-scale models, which will be referred to hereafter as the KC scheme. A freezing mechanism for internally mixed aerosols containing both soluble and insoluble material was included, which was referred to as the DHF mode. The DHF mode suggests that ice nucleation may start on the surface of the insoluble substance of an aerosol

ACPD
11, 14339–14381, 2011

particle embedded in a cloud droplet that has formed on the soluble substance of the same particle. This scenario could be applied to all internally mixed aerosols including dust particles. The classical formulation for condensation-freezing mode allows nucleation only at water saturation and assumes the IN is insoluble (Fukuta and Schaller, 1982), whereas the DHF mode considers internally mixed aerosols with both soluble and insoluble material, and allows nucleation at subsaturation over water. In other words, the DHF mode combines the condensation and immersion freezing mode from the classical heterogeneous ice nucleation theory. Results from a parcel model implemented with the scheme showed good agreement with observations (Khvorostyanov and Curry, 2005). Detailed comparison of the KC scheme with measurements made in recent field campaigns, laboratory measurements and several other empirical ice nucleation parameterizations can be found in Curry and Khvorostyanov (2010).

Based on the results from the parcel model simulations, a simple parameterization for the ice crystal concentration as function of temperature (T) and vertical velocity (w) has been derived (Khvorostyanov and Curry, 2005). It is in the form of $N(T,w) = C_g(T_0 - T)^{C_T} w^{C_w}$, where N is the ice crystal concentration in units of l^{-1}, $T_0 = 0\,^{\circ}\mathrm{C}$, and $C_w = 1.41$. When $T > -15\,^{\circ}\mathrm{C}$, $C_g = 0.4 \times 10^{-8}$, and $C_T = 8.0$. When $T \leq -15\,^{\circ}\mathrm{C}$, $C_g = 0.535$, and $C_T = 1.05$. Figure 3 shows the comparison of ice number concentrations predicted by Cooper (1986), Meyers et al. (1992), and the KC schemes. Both the Cooper and Meyer schemes are functions only of temperature. A fixed maximum value of IN is often specified to prevent unreasonable prediction of ice crystals when temperature is extremely low. For example, the maximum number of ice crystals from the Cooper scheme is set to $500\,\mathrm{l}^{-1}$ in the Morrison scheme. On the other hand in the KC scheme, ice crystal concentration is a function of both temperature and vertical velocity. The maximum value of ice crystal concentration is not limited by a prescribed number, but rather by the cloud droplet number concentration that is related to the aerosol concentration. As shown in Fig. 3, if a model grid point has a vertical velocity greater than $10\,\mathrm{cm\,s}^{-1}$ and temperature between $-6\,^{\circ}\mathrm{C}$ to $-35\,^{\circ}\mathrm{C}$, more ice crystals will be predicted by the KC scheme than by the Cooper and Meyers schemes. The strong

ACPD
11, 14339–14381, 2011

dependence of the ice number concentration on vertical velocity is consistent with in situ measurements made during the NAMMA field campaigns (Heymsfield et al., 2009). Hence, the KC scheme produces more ice crystals at a lower altitude in strong updraft cores than the ice nucleation schemes currently employed in the Morrison microphysics parameterization.

3.2 Design of numerical experiments

To examine the effect of dust as CCN and IN on Helene's early development and evaluate the newly-implemented KC scheme, two groups of WRF simulations with various aerosol concentrations were conducted: one group used the original Morrison scheme, and the other used only the KC scheme for heterogeneous ice nucleation. To represent the storm development under a dust-free maritime condition, a Clean simulation was established first with the original Morrison scheme. In the Clean case, a constant aerosol concentration of 100 cm^{-3} was prescribed across the domain. Aerosol particles have a lognormal size distribution with two modes. The mean radius of each mode was 0.023 and 0.08 µm with a standard deviation of 1.6 and 1.5, respectively. This is consistent with the aerosol size distributions observed over the tropical ocean (Heintzenberg et al., 2000).

To represent the storm development in dust conditions, the aerosol concentration was varied within a certain range in the group of simulations with the original Morrison scheme and the group of simulations with the KC scheme. In the vertical, dust particles were placed in a layer between 1 and 5 km a.s.l. based on the CALIPSO lidar observations (Fig. 2b). The dust particles were assumed to be horizontally distributed since a complete dust emission, transportation and depletion module is still under examination. This assumption may overestimate the storm area affected by dust. Dust size distribution was assumed to have two modes with the mean radius of 0.05 and 0.35 µm and standard deviation of 1.85 and 2.5, respectively, which was based on observations made in the SAL during the NAMMA (Zipser et al., 2009; Chen et al., 2010). Below and above the dust layer, aerosol properties in the Clean simulation were used

ACPD
11, 14339–14381, 2011

to provide the background conditions. According to the NAMMA observations made in the SAL, the dust total number concentration was primarily between 300 to 800 cm^{-3} (Chen et al., 2010). The averaged number concentration for aerosol particles with a diameter greater than 10 nm was 350 cm^{-3}. Therefore, within each group of simulations, dust concentration was varied from 300, 350, to 400 cm^{-3} to represent an average dust loading, and the doubled values 600, 700, to 800 cm^{-3} to represent a heavy dust loading. Simulations using the original Morrison scheme were named "Dust_300", "Dust_350", "Dust_400", "Dust_600", "Dust_700" and "Dust_800", with the number after "Dust_" denoting the total dust concentration. Dust aerosols can be activated as CCN following Abdul-Razzak et al. (1998) and Abdul-Razzak and Ghan (2000). Simulations with the KC scheme were named in the same manner except a suffix of "_KC" was used. In this group of simulations, cloud droplets formed from activated dust particles can freeze through the KC scheme. The grid-scale velocities were used in the KC scheme to derive the nucleation rate, which were found to be comparable to observations made in TCs (Black et al., 1996; Heymsfield et al., 2010). Since the dust aerosol distribution is horizontally homogeneous and does not change with time, activation of dust particles may be overestimated. In addition, since dust particles were constrained below 5 km and were not able to be transported aloft, the process of dust particles acting directly as IN will not be included, which may lead to an underestimation of ice nucleation.

4 Results

4.1 Impact of dust acting as CCN and IN on storm intensity and track

During the three-day period considered here, the pre-Helene MCS first became a tropical depression and then a tropical storm. Since the wind speed and MSLP analysis were only recorded when the MCS reached tropical depression stage, other variables are needed to track the storm intensity prior to that stage. Therefore, we used

ACPD
11, 14339–14381, 2011

the integrated kinetic energy (IKE) introduced by Powell et al. (2007), which is an integration of surface kinetic energy over the storm domain. The IKE is particularly useful for monitoring the pre-Helene MCS development as it provides a continuous measure of the storm intensity before and after the storm showed a closed circulation center. The IKE for each simulation was calculated by summing the square of 10-m wind speed (i.e., wind speed at 10 m above surface) over an area of 750 km by 750 km (150 by 150 grids) centered at the storm and within a 1-m thick layer. Figure 4 shows the evolution of IKE for the two groups of simulations (with the original Morrison scheme and with the KC scheme) during the 60 h period when the inner Domain 2 was turned on. In both cases , IKE started to diverge at 20 h and reached the largest difference at the end of the simulation. The maximum difference in IKE between the Clean and all dust cases was 7.3 TJ (a 14.3 % deviation from the Clean) for simulations with the original Morrison scheme and 10.7 TJ (a 21 % deviation from the Clean) for simulations with the KC scheme. Thus, the storm intensity was more sensitive to the aerosol concentration in simulations with the KC scheme. The final MSLP ranged from 986 hPa (Clean) to 1005 hPa (Dust_350_KC). In both groups, we found non-monotonic dependence of IKE on dust concentration.

Numerical simulations of TCs are very sensitive to initial conditions (Sippel and Zhang, 2008, 2010). Sensitivity experiments by varying the simulation starting time have been conducted. For example, the final MSLP from simulations with the original Morrison scheme initialized 6 h later ranged from 989 (Clean aerosol) to 995 hPa (aerosol concentration of 400 cm^{-3}). For the group with the KC scheme initialized 6 h later, the final MSLP ranged from 988 (aerosol concentration of 400 cm^{-3}) to 1002 hPa (aerosol concentration of 800 cm^{-3}). The storm intensity evolution was sensitive to the initial conditions. Again, non-monotonic dependence of IKE on dust concentration was found. Clean was not always the strongest storm and adding more aerosols did not necessarily lead to a weaker storm. This is consistent with conclusions from the idealized TC simulations (Zhang et al., 2007, 2009; Zhang, 2008) that no clear monotonic relationship of dust concentration with TC intensity can be drawn.

ACPD
11, 14339–14381, 2011

Regarding the storm track, all simulated storms moved at a slower speed than the observed storm. Different combinations of physical parameterizations were tested, but none was able to increase the storm speed. The slow storm movement was most likely caused by biases in the steering flow simulated in the inner domain. At the end of the simulation period (00:00 UTC 14 September), the observed storm was located at (31.9° W, 12.9° N). The storms from simulations with the original Morrison scheme reached a final location at (27.5° W, 14.7° N). The storms from simulations with the KC scheme reached at (28.5° W, 14.2° N). By modifying the heterogeneous freezing mode in the microphysics scheme, storm final location was changed by 1° in the longitude and 0.5° in the latitude. The changes in the final location were likely caused by variations in the vertical wind shear induced by asymmetry of convection (Wu and Wang, 2000).

4.2 Impact of dust acting as CCN and IN on hydrometeors distribution

The initial mechanism for dust aerosols to affect the cloud development is through CCN activation to form cloud droplets. By acting as CCN, more dust led to higher cloud droplet number concentration in all simulations. Averaged over the entire 60 h, the cloud droplet number concentration, for instance, at 2 km just above the cloud base was 34, 52, 55, 57, 64, 67, and 77 cm^{-3} for Clean, Dust_300, Dust_350, Dust_400, Dust_600, Dust_700, and Dust_800, respectively. Similarly, the cloud number concentration for Dust_300_KC, Dust_350_KC, Dust_400_KC, Dust_600_KC, Dust_700_KC, and Dust_800_KC was 34, 52, 56, 57, 64, 68, and 72 cm^{-3}, respectively. When cloud droplets reach the 0 °C level at about 4.5 km, ice particles can start to form through heterogeneous freezing. The supercooled cloud droplets that reach the 10 km level with temperature of −40 °C will immediately freeze into ice particles through homogeneous freezing.

To evaluate the ice production in the pre-Helene MCS, observations from the Cloud Profiling Radar (CPR) onboard CloudSat were used. The CPR is a 94-GHz nadir-viewing radar that measures the power backscattered by clouds as a function of distance from the radar (Stephens et al., 2002). At 14:54 UTC 11 September, CPR

ACPD
11, 14339–14381, 2011

captured the frontal edge of the pre-Helene MCS (Fig. 5a), when the dust layer was approaching the storm from the north and northwest (Fig. 1a). Seen from the retrieved radar reflectivity (Fig. 5b), the cloud top near the frontal edge reached up to 14 km, and a bright band formed by melting snow and graupel can be seen at 4.5 km. High ice water content (IWC) with a value greater than 0.8 g m^{-3} was concentrated within a layer from 7 to 10 km (Fig. 5c), which was below the homogeneous freezing level at 10 km with temperature of −40 °C. The estimated total ice number concentration for high IWC region was more than 300 l^{-1} (Fig. 5d).

To evaluate the effect of the KC ice nucleation scheme, Fig. 6 compares the vertical cross sections of the simulated ice and cloud properties along the CloudSat path for Clean and Dust_350_KC. This case represents the average aerosol concentration (350 cm^{-3}) in the SAL observed during NAMMA (Chen et al., 2010). Since the ice properties obtained along a single line may not represent the ice distribution in the entire storm, domain averaged ice crystal water content and number concentration at this time were calculated and shown in Fig. 7. Here, the Clean was used to represent the group of simulations with the original Morrison scheme as the difference in ice properties among simulations were found to be very small as illustrated in Fig. 7a and b. A clean environment is also assumed as the default condition in many TC forecast models. For the ice crystal production, the original Morrison scheme tends to produce a large area with extremely high ice crystal number concentration above 10 km away from the updraft cores (Fig. 6e), leading to more prominent anvil clouds (Fig. 6a and c). This was due to the fact that the heterogeneous nucleation parameterizations in the original Morrison scheme are mainly function of temperature. On the other hand, because the ice production in the KC scheme depends on both temperature and vertical velocity, the ice crystal water content and number concentration were highly correlated with vertical velocity (Fig. 6d and f), which is more consistent with NAMMA observations (Heymsfeld et al., 2009). Below the melting level, the cloud droplet concentration was higher in Dust_350_KC (Fig. 6l) than in Clean (Fig. 6k) due to the effect of dust aerosols acting as CCN. Above the melting level in the strong updraft cores, cloud

ACPD
11, 14339–14381, 2011

droplet concentration in Dust_350_KC was reduced since the KC scheme tends to convert cloud droplets into ice crystals through the DHF mode due to the effect of dust acting as IN.

To compare with the CloudSat retrieval, water content and number concentration from ice crystal, snow, and graupel were added together to obtain the total IWC and number concentration. The total IWC was dominated by contribution from snow and graupel, while the ice number concentration was dominated by contribution from ice crystals. Compared to the CloudSat retrieval (Fig. 5c and d), the original Morrison scheme significantly overestimated the amount of IWC (Fig. 6g), although it should be noted that the CloudSat retrieval below 7 km could be greatly affected by the attenuation of CPR signals due to snow and graupel formed in tropical deep convection (Protat et al., 2009). The original Morrison scheme also overestimated the ice number concentration above 10 km and underestimated it below this level (Fig. 6i). The KC scheme reduced the amount of ice above 10 km (Figs. 6h and 7c) and the area of high ice number concentration outside of the updraft cores (Fig. 6j), which led to a slightly lower cloud top height. Averaged over the entire storm, the KC scheme produced fewer ice crystals above 9 km and more ice crystals between 7 and 9 km (Fig. 7d) than the simulations with the original Morrison scheme (Fig. 7b). The KC scheme tends to suppress homogeneous freezing at higher altitudes and promote heterogeneous nucleation at lower altitudes. The ice production in the KC scheme was highly correlated with the vertical velocity, and the amount of high clouds outside of the updraft cores was reduced. In both groups of simulations, the ice number concentration was significantly reduced below 10 km (Figs. 6i and j and 7b and d). By conducting sensitivity tests with selected ice to snow processes turned off, the sharp reduction was found primarily due to aggressive conversion of ice to snow by accretion in the Morrison scheme, with the autoconversion process playing a minor role.

ACPD
11, 14339–14381, 2011

4.3 Impact of dust acting as CCN and IN on cloud top temperature

It has been found that high clouds associated with strong convection often precede TC intensification (Steranka et al., 1986). Using a coupled ocean-atmosphere model, Emanuel (1999) derived an equation to calculate the TC potential intensity as a function of cloud top temperature, which shows that if all other parameters remain the same, an increase in cloud top temperature (T_0) implies a lower storm potential intensity. Based on this theory, a new technique was developed to estimate the TC intensity using high resolution observations of cloud top temperature and cloud top height (Luo et al., 2008).

To quantify the effect of the KC scheme on high cloud development, simulated cloud top temperature distributions were compared with retrievals from two MODIS overpasses on 11 and 12 September. On 11 September, the pre-Helene MCS moved to the edge of the African coast (Fig. 8a). The frequency of occurrence of the cloud top temperatures peaked at 218 K (Fig. 8d), which appears in color blue in Fig. 8a. The simulated cloud top temperature did not differ significantly within each group (Fig. 8d and e). Therefore, horizontal distributions of cloud top temperature from Clean and Dust_350_KC were chosen to represent the two groups, respectively (Fig. 8b and c). A clean environment is also the default condition in many TC forecast models. Although the simulated storm intensities from both groups (Fig. 4) were very similar at this time, the difference in the cloud top temperature distribution between the two groups was already noticeable (Fig. 8d and e). Simulations with the original Morrison scheme produced more area of high clouds with cloud top temperature lower than 215 K, and less area of low clouds with cloud top temperature higher than 215 K. Simulations with the KC scheme predicted less area of high clouds and more area of low clouds, which is consistent with the analysis of ice properties (Figs. 6 and 7). Another MODIS image was available on 12 September (Fig. 9a), when the dust layer can be seen approaching the storm from north and northwest (Fig. 2a). Similarly, simulations with the KC scheme predicted a smaller area of high clouds and a larger area of low clouds compared to the original Morrison scheme (Fig. 9d and e). Even though the storm intensities were

ACPD
11, 14339–14381, 2011

similar at both times, storm structures have already shown consistent difference between the group of simulations with the original Morrison scheme and the group with KC scheme.

To further examine the effect of the KC scheme on cloud top temperature distribution, two sensitivity experiments were conducted by turning on either homogeneous or heterogeneous ice nucleation parameterizations in Dust_350_KC. The cloud top temperature distributions from these two simulations are shown in Fig. 8e. Simulation with only homogeneous freezing produced a larger area with high clouds and a smaller area with low clouds, while simulation with only heterogeneous freezing (the KC scheme) produced a smaller area with high clouds and more area with low clouds.

Figure 10 shows the Meteosat IR imagery, cloud top temperature and outgoing longwave radiation (OLR) distribution from Clean, Dust_350, and Dust_350_KC at 00:00 UTC 14 September. Significant differences in the storm size and cloud top temperature distribution (hence the OLR) can be seen among the simulations with the original Morrison scheme versus the KC scheme. Consistent with the previous analysis of ice production and cloud top temperature, the original Morrison scheme produced more area of high clouds with cloud top temperature lower than −55 °C, whereas the KC scheme produced more area of low clouds with increased OLR. The enhanced OLR also has a cooling effect on the atmosphere (Min and Li, 2010). Modification in the ice parameterization has led to changes in the cloud structure and the radiative energy budget of the storm.

4.4 Impact of dust acting as CCN and IN on precipitation

To evaluate the simulated precipitation distributions, near surface rainfall rates (2A12) obtained by the TRMM Microwave Imager (TMI) were analyzed and compared with the corresponding model output. The TRMM TMI captured the pre-Helene MCS twice on 12 September (Figs. 11a and 12a). The simulated surface rain rate distributions for Clean and Dust_350_KC shown in Figs. 11 and Fig. 12 were obtained at the time when the simulated storm moved to a similar location as the observed one. Difference

ACPD
11, 14339–14381, 2011

in precipitation rates among simulations in both groups was not significant (Figs. 11d, 11e, 12d and 12e), except for the area with rainrate of 1 mm h^{-1}. At both times, simulations with dust aerosols and KC scheme produced 25 % to 30 % area with rainrate of 1 mm h^{-1}, which is slightly more than the 24 % of area produced by the Clean simulation. The lack of sensitivity of surface rainrate to the aerosol concentration may be related to the saturation adjustment, a procedure often used in a bulk microphysics scheme that converts all extra water vapor into cloud water regardless of the cloud number concentration. In general, the simulated precipitation distributions agreed well with observations, except that the simulations tend to underpredict the area of rain rate between 2 to 10 mm h^{-1} but overestimate the area with rain rate higher than 10 mm h^{-1}. The total precipitation integrated over the entire three days shows very little variation with aerosol concentration and less than 10 % difference between the original Morrison versus the KC scheme, with simulations using the original Morrison scheme producing slightly more total precipitation. This lack of the impact of dust on total precipitation amount is consistent with the results from idealized simulations (Zhang et al., 2007, 2009) and other previous studies (Levin et al., 2005; Yin and Chen, 2007).

4.5 Impact of dust acting as CCN and IN on latent heat release

Varying aerosol concentration and implementing the KC heterogeneous ice nucleation scheme ultimately affected the storm evolution through modifying the distribution of latent heat. Figure 13 shows the averaged latent heating profiles from the simulations with the original Morrison scheme and the KC scheme. The latent heating profiles from two overpasses of TRMM TMI (2A12) are also presented in Fig. 13. Although significant variability in heating profiles can be seen among simulations at the selected TRMM overpasses (Fig. 13a, b, e and f), all simulations reproduced the two heating maxima observed by TRMM: one between 1 and 4 km, and the other between 5 and 10 km. If only accounting for the latent heating within the strong updraft cores (vertical velocity greater than 1 m s^{-1}), simulations with the KC scheme produced more latent heat between 4 and 10 km than the original Morrison scheme (Fig. 13c and g),

ACPD
11, 14339–14381, 2011

which was between the melting level and the homogeneous freezing level. This is expected from the KC scheme, which promotes more ice to form through the DHF mode in strong updrafts. However when averaged over the entire 60 h period, simulations with the KC scheme consistently produced less heating than Clean from 1 to 12 km (Fig. 13h) and simulations with the original Morrison scheme did not show significant difference (Fig. 13d). This is consistent with the fact that simulations with the original Morrison scheme did not show significant difference in storm intensity (Fig. 4a), while simulations with the KC scheme produced relatively weaker storms for this particular group of simulation (Fig. 4b). The averaged latent heating rate was non-monotonically related with the dust concentration using either parameterization. The lack of sensitivity of the averaged total latent heating profile and total precipitation to aerosol concentration indicates that the storm dynamics and total moisture supply (which is abundant over tropical ocean) maybe more important factors in determining these quantities.

Varying aerosol concentration and introducing the KC scheme not only modified the vertical profile of latent heating but also changed its horizontal distribution. At the end of the simulation, the azimuthally averaged latent heating rate and vertical velocity distribution in the Clean, Dust_350_KC, and Dust_700_KC cases were distinctively different (Fig. 14). The latent heating and vertical velocity maxima were located near 25 km from the storm center in the Clean case (Fig. 14a and d) and 50 km in Dust_350_KC (Fig. 14b and e) and Dust_700_KC (Fig. 14c and f). Even though the IKE of Dust_700_KC was only 6 % less than the Clean case at this time, their latent heat and vertical velocity distributions were quite different. The KC scheme accounting for dust's ability as CCN and IN has modified the storm intensity, track, hydrometeor distribution, cloud structure, radiative energy budget and precipitation distribution and latent heating structure during the three-day simulation.

ACPD
11, 14339–14381, 2011

5 Conclusions and discussion

The impact of Saharan dust acting as both CCN and IN on Hurricane Helene's early development was examined by performing a series of numerical simulations using the WRF model. An ice nucleation parameterization, which accounts for the DHF mode based on Khvorostyanov and Curry (2000, 2004, 2005) depending upon both air temperature and vertical velocity (an implicit dependence on supersaturation), was incorporated into the Morrison microphysics scheme within WRF. Satellite observations from MODIS, CALIPSO, CloudSat, and TRMM were utilized to examine the distributions and properties of dust particles, hydrometeors, precipitation, and latent heat release, as well as to constrain and evaluate the WRF model. Two groups of simulations with varying dust concentration using either the original Morrison scheme or KC scheme were presented in details.

Dust particles led to an increase in the cloud droplet number concentration in both groups. The KC scheme tends to promote heterogeneous nucleation at lower altitudes and suppress homogeneous freezing at higher altitudes. The ice production was highly correlated with the vertical velocity and the amount of high clouds outside of the updraft cores was reduced, which is more consistent with the CloudSat retrieval and NAMMA observations. This suggests that the ice nucleation parameterization as a simple function of temperature currently used in the Morrison scheme (and many other microphysics schemes) may not accurately depict the physical processes occurring in the TCs affected by dust. Comparisons with CloudSat and MODIS retrieval suggest that the KC scheme produced more low clouds with high cloud top temperature as it tends to promote ice formation at lower altitudes. Sensitivity tests by turning off the homogeneous or heterogeneous freezing process further confirmed this conclusion. Simulations with the KC scheme tend to produce more ice crystals and latent heat in strong updraft cores as more cloud droplets formed on dust particles that froze through the DHF mode, which may potentially enhance lightning activities as observed during NAMMA. The sensitivity of these conclusions to initial condition uncertainty was confirmed by simulations conducted with different initialization times.

ACPD
11, 14339–14381, 2011

In our WRF simulations, we assumed that the dust plume was horizontally homogeneous, and no dust radiative feedbacks were considered. Even in this case, storm intensity and latent heating rates were non-monotonically related to dust concentrations. The complex impact of dust on microphysical and radiative processes and the non-linear nature of convection make it difficult to define a simple relationship between dust and storm intensity. We plan to further explore this problem by improving representations of three-dimensional dust fields and activation of dust as CCN, as well as inclusion of the dust radiative impact in the future. Nevertheless, this study shows that atmospheric aerosols such as dust acting as CCN and IN can influence the early development of TC by inducing changes in the storm intensity, track, hydrometeor properties, cloud top temperature (hence the radiative energy budget) and latent heating distribution. Traditionally, the evolution of TC intensity is considered mainly depending on the storm initial intensity, the thermodynamic state of the atmosphere, and the heat exchange with the upper layer of the ocean (Emanuel, 1999). In many TC forecast models, a clean background condition is often assumed. Our study shows that aerosols should be considered as another variable that can affect individual TC's development. Future improvement in the representation of the atmospheric aerosols in cloud microphysical parameterizations has the potential to lead to better prediction of the track, intensity, and structure of a TC.

Acknowledgements. This research was supported by the National Science Foundation (Grant AGS-1064346) and NASA CloudSat/CALIPSO Program (Grant NNX07AQ78G). The authors would like to thank V. I. Khvorostyanov and H. Morrison for providing the ice nucleation parameterization and microphysics scheme and Y. Deng for providing the computing facilities. The authors are grateful to V. I. Khvorostyanov, H. Morrison, Y. Deng, G. Chen, J. Knaff and C. Twohy for the many helpful discussions and data they provided, and S. Ryan for assistance with the manuscript.

ACPD
11, 14339–14381, 2011

References

Abdul-Razzak, H. and Ghan, S. J.: A parameterization of aerosol activation: 2. Multiple aerosol types, J. Geophys. Res.,105, 6837–6844, 2000.

Abdul-Razzak, H., Ghan, S. J., and Rivera-Carpio, C.: A parameterization of aerosol activation: 1. single aerosol type, J. Geophys. Res., 103, 6123–6131, 1998.

Ansmann, A., Tesche, M., Althausen, D., Müller, D., Seifert, P., Freudenthaler, V., Heese, B., Wiegner, M., Pisani, G., Knippertz, P., and Dubovik, O.: Influence of Saharan dust on cloud glaciation in southern Morocco during the Saharan Mineral Dust Experiment, J. Geophys. Res., 113, D04210, doi:10.1029/2007JD008785, 2008.

Bigg, E. K.: The supercooling of water, P. Phys. Soc. Lond. B, 66, 688–694, 1953.

Black, M. L., Burpee, R. W., and Marks, F. D.: Vertical motion characteristics of tropical cyclones determined with airborne Doppler radial velocities, J. Atmos. Sci., 53, 1887–1909, 1996.

Braun, S. A.: Reevaluating the role of the Saharan Air Layer in Atlantic tropical cyclogenesis and evolution, Mon. Weather Rev., 138, 2007–2037, doi:10.1175/2009MWR3135.1, 2010.

Carlson, T. N. and Prospero, J. M.: The large-scale movement of Saharan air outbreaks over the northern equatorial Atlantic, J. Appl. Meteorol., 11, 283–297, 1972.

Chen, S.-H., Wang, S.-H., and Waylonis, M.: Modification of Saharan air layer and environmental shear over the eastern Atlantic Ocean by dust-radiation effects, J. Geophys. Res., 115, D21202, doi:10.1029/2010JD014158, 2010.

Chen, G., Ziemba, L. D., Chu, D. A., Thornhill, K. L., Schuster, G. L., Winstead, E. L., Diskin, G. S., Ferrare, R. A., Burton, S. P., Ismail, S., Kooi, S. A., Omar, A. H., Slusher, D. L., Kleb, M. M., Reid, J. S., Twohy, C. H., Zhang, H., and Anderson, B. E.: Observations of Saharan dust microphysical and optical properties from the Eastern Atlantic during NAMMA airborne field campaign, Atmos. Chem. Phys., 11, 723–740, doi:10.5194/acp-11-723-2011, 2011.

Connolly, P. J., Möhler, O., Field, P. R., Saathoff, H., Burgess, R., Choularton, T., and Gallagher, M.: Studies of heterogeneous freezing by three different desert dust samples, Atmos. Chem. Phys., 9, 2805–2824, doi:10.5194/acp-9-2805-2009, 2009.

Cooper, W. A.: Ice initiation in natural clouds, Precipitation enhancement – a scientific challenge, Meteor. Mon., 43, 29–32, 1986.

Curry, J. A. and Khvorostyanov, V. I.: Assessment of parameterizations of heterogeneous ice nucleation in cloud and climate models, Atmos. Chem. Phys. Discuss., 10, 2669–2710,

ACPD
11, 14339–14381, 2011

doi:10.5194/acpd-10-2669-2010, 2010.
DeMott, P. J., Sassen, K., Poellet, M. R., Baumgardner, D., Rogers, D. C., Brooks, S. D., Prenni, A. J., and Kreidenweis, S. M.: African dust aerosols as atmospheric ice nuclei, Geophys. Res. Lett., 30(14), 1732, doi:10.1029/2003GL017410, 2003.
DeMott, P. J., Sassen, K., Poellet, M. R., Baumgardner, D., Rogers, D. C., Brooks, S. D., Prenni, A. J., and Kreidenweis, S. M.: Correction to "African dust aerosols as atmospheric ice nuclei", Geophys. Res. Lett., 36, L07808, doi:10.1029/2009GL037639, 2009.
Diehl, K. and Wurzler, S.: Heterogeneous drop freezing in the immersion mode: Model calculations considering soluble and insoluble particles in the drops, J. Atmos. Sci., 61(16), 2063–2072, 2004.
Dunion, J. P. and Velden, C. S.: The impact of the Saharan Air Layer on Atlantic tropical cyclone activity, B. Am. Meteorol. Soc., 85, 353–365, 2004.
Eidhammer, T., DeMott, P. J., Prenni, A. J., Petters, M. D., Twohy, C. H., Rogers, D. C., Stith, J., Heymsfield, A., Wang, Z., Pratt, K. A., Prather, K. A., Murphy, S. M., Seinfeld, J. H., Subramanian, R., and Kreidenweis, S. M.: Ice initiation by aerosol particles: measured and predicted ice nuclei concentrations versus measured ice crystal concentrations in an orographic wave cloud, J. Atmos. Sci., 67, 2417–2436, doi:10.1175/2010JAS3266.1, 2010.
Emanuel, K. A.: Thermodynamic control of hurricane intensity, Nature, 401, 665–669, 1999.
Evan, A. T., Dunion, J., Foley, J. A., Heidinger, A. K., and Velden, C. S.: New evidence for a relationship between Atlantic tropical cyclone activity and African dust outbreaks, Geophys. Res. Lett., 33, L19813, doi:10.1029/2006GL026408, 2006.
Evan, A. T., Vimont, D. J., Heidinger, A. K., Kossin, J. P., and Bennartz, R.: The role of aerosols in the evolution of tropical Atlantic Ocean temperature anomalies, Science, 324, 778–781, doi:10.1126/science.1167404, 2009.
Field, P. R., Möhler, O., Connolly, P., Krämer, M., Cotton, R., Heymsfield, A. J., Saathoff, H., and Schnaiter, M.: Some ice nucleation characteristics of Asian and Saharan desert dust, Atmos. Chem. Phys., 6, 2991–3006, doi:10.5194/acp-6-2991-2006, 2006.
Fukuta, N. and Schaller, R. C.: Ice nucleation by aerosol particles: theory of condensation-freezing nucleation, J. Atmos. Sci., 39, 648–655, 1982.
Guedalia, D., Estournel, C., and Vehil, R.: Effects of Sahel dust layers upon nocturnal cooling of the atmosphere (ECLATS Experiment), J. Clim. Appl. Meteorol., 23, 644–650, 1984.
Heintzenberg, J., Covert, D. C., and van Dingenen, R.: Size distribution and chemical composition of marine aerosols: a compilation and review, Tellus B, 52(4), 1104–1122, 2000.

ACPD
11, 14339–14381, 2011

Heymsfield, A. J., Bansemer, A., Heymsfield, G., and Fierro, A. O.: Microphysics of maritime tropical convective updrafts at temperatures from −20 °C to −60 °C, J. Atmos. Sci., 66, 3530–3562, 2009.
Heymsfield, G. M., Tian, L., Heymsfield, A. J., Li, L., and Guimond, S.: Characteristics of deep tropical and subtropical convection from nadir-viewing high-altitude airborne Doppler radar, J. Atmos. Sci., 67, 285–308, 2010.
Isono, K., Komabayasi, M., and Ono, A.: The nature and origin of ice nuclei in the atmosphere, J. Meteorol. Soc. Jpn., 37, 211–233, 1959.
Jenkins, G. S. and Pratt, A.: Saharan dust, lightning and tropical cyclones in the eastern tropical Atlantic during NAMMA-06, Geophys. Res. Lett., 35, L12804, doi:10.1029/2008GL033979, 2008.
Jenkins, G. S., Pratt, A. S., and Heymsfield, A.: Possible linkages between Saharan dust and tropical cyclone rain band invigoration in the eastern Atlantic during NAMMA-06, Geophys. Res. Lett., 35, L08815, doi:10.1029/2008GL034072, 2008.
Jones, T. A., Cecil, D. J., and Dunion, J.: The environmental and inner-core conditions governing the intensity of Hurricane Erin (2007), Weather Forecast., 22, 708–725, 2007.
Karyampudi, V. M. and Carlson, T. N.: Analysis and numerical simulations of the Saharan air layer and its effect on easterly wave disturbances, J. Atmos. Sci., 45, 3102–3136, 1988.
Karyampudi, V. M. and Pierce, H. F.: Synoptic-scale influence of the Saharan air layer on tropical cyclogenesis over the eastern Atlantic, Mon. Weather Rev., 130, 3100–3128, 2002.
Karyampudi, V. M., Palm, S. P., Reagen, J. A., Fang, H., Grant, W. B., Hoff, R. M., Moulin, C., Pierce, H. F., Torres, O., Browell, E. V., and Melfi, S. H.: Validation of the Saharan dust plume conceptual model using Lidar, Meteosat, and ECMWF data, B. Am. Meteorol. Soc., 80, 1045–1074, 1999.
Kaufman, Y. J., Koren, I., Remer, L. A., Rosenfeld, D., and Rudich, Y.: The effect of smoke, dust, and pollution aerosol on shallow cloud development over the Atlantic ocean, P. Natl. Acad. Sci., 102, 11207–11212, 2005.
Khain, A., Cohen, N., Lynn, B., and Pokrovsky, A.: Possible aerosol effects on lightning activity and structure of hurricanes, J. Atmos. Sci., 65, 3652–3677, 2008.
Khain, A., Lynn, B., and Dudhia, J.: Aerosol effects on intensity of landfalling Hurricanes as seen from simulations with the WRF model with spectral bin microphysics, J. Atmos. Sci., 67, 365–384, 2010.
Khvorostyanov, V. I. and Curry, J. A.: A new theory of heterogeneous ice nucleation for appli-

ACPD
11, 14339–14381, 2011

cation in cloud and climate models, Geophys. Res. Lett., 27, 4081–4084, 2000.
Khvorostyanov, V. I. and Curry, J. A.: The theory of ice nucleation by heterogeneous freezing of deliquescent mixed CCN. Part I: Critical radius, energy, and nucleation rate, J. Atmos. Sci., 61(22), 2676–2691, 2004.
Khvorostyanov, V. I. and Curry, J. A.: The theory of ice nucleation by heterogeneous freezing of deliquescent mixed CCN. Part II: Parcel model simulation, J. Atmos. Sci., 62(2), 261–285, 2005.
Köhler, H.: The nucleus and growth of hygroscopic droplets, T. Faraday Soc., 32, 1152–1161, 1936.
Kumar, P., Sokolik, I. N., and Nenes, A.: Parameterization of cloud droplet formation for global and regional models: including adsorption activation from insoluble CCN, Atmos. Chem. Phys., 9, 2517–2532, doi:10.5194/acp-9-2517-2009, 2009a.
Kumar, P., Nenes, A., and Sokolik, I. N.: Importance of adsorption for CCN activity and Hygroscopic properties of mineral dust aerosol, Geophs. Res. Lett., 36, L24804, doi:10.1029/2009GL040827, 2009b.
Lau, K. M. and Kim, J. M.: How nature foiled the 2006 hurricane forecasts, EOS Trans., 88(9), 105–107, 2007.
Levin, Z., Ganor, E., and Gladstein, V.: The effects of desert particles coated with sulfate on rain formation in the eastern Mediterranean, J. Appl. Meteorol., 35, 1511–1523, 1996.
Levin, Z., Teller, A., Ganor, E., and Yin, Y.: On the interactions of mineral dust, sea salt particles and clouds: A measurement and modeling study from the Mediterranean Israeli Dust Experiment campaign, J. Geophys. Res., 110, D20202, doi:10.1029/2005JD005810, 2005.
Li, R. and Min, Q.-L.: Impacts of mineral dust on the vertical structure of precipitation, J. Geophys. Res., 115, D09203, doi:10.1029/2009JD011925, 2010.
Luo, Z., Stephens, G. L., Emanuel, K. A., Vane, D. G., Tourville, N., and Haynes, J. M.: On the use of CloudSat and MODIS data for estimating hurricane intensity, IEEE Geosci. Remote S., 5, 13–16, 2008.
Mahowald, N. M. and Kiehl, L. M.: Mineral aerosol and cloud interactions, Geophys. Res. Lett., 30(9), 1475, doi:10.1029/2002GL016762, 2003.
Meyers, M. P., DeMott, P. J., and Cotton, W. R.: New primary ice-nucleation parameterizations in an explicit cloud model, J. Appl. Meteorol., 31, 708–721, 1992.
Min, Q. and Li, R.: Longwave indirect effect of mineral dusts on ice clouds, Atmos. Chem. Phys., 10, 7753–7761, doi:10.5194/acp-10-7753-2010, 2010.

ACPD
11, 14339–14381, 2011

Min, Q.-L., Li, R., Lin, B., Joseph, E., Wang, S., Hu, Y., Morris, V., and Chang, F.: Evidence of mineral dust altering cloud microphysics and precipitation, Atmos. Chem. Phys., 9, 3223–3231, doi:10.5194/acp-9-3223-2009, 2009.

Morrison, H. and Pinto, J. O.: Mesoscale modeling of springtime arctic mixed phase stratiform clouds using a new two-moment bulk microphysics scheme, J. Atmos. Sci., 62, 3683–3704, 2005.

Morrison, H., Curry, J. A., and Khvorostyanov, V. I.: A new double-moment microphysics scheme for application in cloud and climate models. Part I: Description, J. Atmos. Sci., 62, 1665–1677, 2005.

Petters, M. D. and Kreidenweis, S. M.: A single parameter representation of hygroscopic growth and cloud condensation nucleus activity, Atmos. Chem. Phys., 7, 1961–1971, doi:10.5194/acp-7-1961-2007, 2007.

Phillips, V. T. J., DeMott, P. J., and Andronache, C.: An empirical parameterization of heterogeneous ice nucleation for multiple chemical species of aerosol, J. Atmos. Sci., 65, 2757–2783, doi:10.1175/2007JAS2546.1, 2008.

Powell, M. D. and Reinhold, T. A.: Tropical cyclone destructive potential by integrated kinetic energy, B. Am. Meteorol. Soc., 88, 513–526, 2007.

Pratt, K. A., DeMott, P. J., French, J. R., Wang, Z., Westphal, D. L., Heymsfield, A. J., Twohy, C. H., Prenni, A. J., and Prather, K.A: In situ detection of biological particles in cloud ice-crystals, Nat. Geosci., 2, 398–401, doi:10.1038/ngeo521, 2009.

Protat, A., Bouniol, D., Delanoë, J., O'Connor, E., May, P. T., Plana-Fattori, A., Hasson, A., Görsdorf, U., and Heymsfield, A. J.: Assessment of CloudSat reflectivity measurements and ice cloud properties using ground-based and airborne cloud radar observations, J. Atmos. Ocean. Tech., 26, 1717–1741, 2009.

Pruppacher, H. R. and Klett, J. D.: Microphysics of Clouds and Precipitation, 2nd Edition, Kluwer, Dordrecht, Netherlands, 1997.

Reale, O., Lau, W. K., Kim, K.-M., and Brin, E.: Atlantic tropical cyclogenetic processes during SOP-3 NAMMA in the GEOS-5 global data assimilation and forecast system, J. Atmos. Sci., 66, 3563–3578, 2009.

Rosenfeld, D., Rudich, Y., and Lahav, R.: Desert dust suppressing precipitation: a possible desertification feedback loop, P. Natl. Acad. Sci., 98(11), 5975– 5980, 2001.

Rosenfeld, D., Khain, A., Lynn, B., and Woodley, W. L.: Simulation of hurricane response to suppression of warm rain by sub-micron aerosols, Atmos. Chem. Phys., 7, 3411–3424,

ACPD
11, 14339–14381, 2011

doi:10.5194/acp-7-3411-2007, 2007.
Sassen, K.: Indirect climate forcing over the western US from Asian dust storms, Geophys. Res. Lett., 29, 1465, doi:10.1029/2001GL014051, 2002.
Sassen, K., DeMott, P. J., Prospero, J. M., and Poellot, M. R.: Saharan dust storms and indirect aerosol effects on clouds: CRYSTAL-FACE results, Geophys. Res. Lett., 30(12), 1633, doi:10.1029/2003GL017371, 2003.
Shu, S. and Wu, L.: Analysis of the influence of Saharan air layer on tropical cyclone intensity using AIRS/Aqua data, Geophys. Res. Lett., 36, L09809, doi:10.1029/2009GL037634, 2009.
Sippel, J. A. and Zhang,F.: A probabilistic analysis of the dynamics and predictability of tropical cyclogenesis, J. Atmos. Sci., 65, 3440–3459, 2008.
Sippel, J. A. and Zhang, F.: Factors affecting the predictability of hurricane Humberto (2007), J. Atmos. Sci., 63, 1759–1778, 2010.
Sokolik, I. N., Winker, D., Bergametti, G., Gillette, D., Carmichael, G., Kaufman, Y., Gomes, L., Schuetz, L., and Penner, J.: Introduction to special section on mineral dust: outstanding problems in quantifying the radiative impact of mineral dust, J. Geophys. Res., 106, 18015–18027, 2001.
Steranka, J., Rodgers, E. B., and Gentry, R. C.: The relationship between satellite measured convective bursts and tropical cyclone intensification, Mon. Weather Rev., 114, 1539–1546, 1986.
Stephens, G. L., Vane, D. G., Boain, R. J., Mace, G. G., Sassen, K., Wang, Z., Illingworth, A. J., O'Connor, E. J., Rossow, W. B., Durden, S. L., Miller, S. D., Austin, R. T., Benedetti, A., and Mitrescu, C.: The CloudSat mission and the A-Train: a new dimension of space-based observations of clouds and precipitation, B. Am. Meteorol. Soc., 83, 1771–1790, doi:10.1175/BAMS-83-12-1771, 2002.
Sun, D., Lau, K. M., and Kafatos, M.: Contrasting the 2007 and 2005 hurricane seasons: evidence of possible impacts of Saharan dry air and dust on tropical cyclone activity in the Atlantic basin, Geophys. Res. Lett., 35, L15405, doi:10.1029/2008GL034529, 2008.
Sun, D., Boybeyi, Z., Yang, C., Yang, R., Lau, W. K. M., Kafatos, M., and Leptoukh, G.: Numerical simulations of the impacts of the Saharan air layer on Atlantic tropical cyclone development, J. Climate, 22, 6230–6250, 2009.
Twohy, C. H., Kreidenweis, S. M., Eidhammer, T., Browell, E. V., Heymsfield, A. J., Bansemer, A. R., Anderson, B. E., Chen, G., Ismail, S., DeMott, P. J., and Van den Heever, S. C.: Saharan dust particles nucleate droplets in eastern Atlantic clouds, Geophys. Res. Lett., 36, L01807,

ACPD
11, 14339–14381, 2011

doi:10.1029/2008GL035846, 2009.
Vali, G.: Nucleation terminology, J. Aerosol Sci., 16, 575–576, 1985.
van den Heever, S. C., Carri, G. G., Cotton, W. R., DeMott, P. J., and Prenni, A. J.: Impacts of nucleating aerosol on Florida storms. Part I: Mesoscale simulations, J. Atmos. Sci., 63, 1752–1775, 2006.
Wiacek, A., Peter, T., and Lohmann, U.: The potential influence of Asian and African mineral dust on ice, mixed-phase and liquid water clouds, Atmos. Chem. Phys., 10, 8649–8667, doi:10.5194/acp-10-8649-2010, 2010.
Wong, S., Dessler, A. E., Mahowald, N. M., Colarco, P. R., and da Silva, A.: Long-term variability in Saharan dust transport and its link to North Atlantic sea surface temperature, Geophys. Res. Lett., 35, L07812, doi:10.1029/2007GL032297, 2008.
Wu, L.: Impact of Saharan air layer on hurricane peak intensity, Geophys. Res. Lett., 34, L09802, doi:10.1029/2007GL029564, 2007.
Wu, L. and Wang, B.: A potential vorticity tendency diagnostic approach for tropical cyclone motion, Mon. Weather Rev., 128, 1899–1911, 2000.
Yin, Y. and Chen, L.: The effects of heating by transported dust layers on cloud and precipitation: a numerical study, Atmos. Chem. Phys., 7, 3497–3505, doi:10.5194/acp-7-3497-2007, 2007.
Zhang, H.: Impact of Saharan dust as CCN on the evolution of an idealized tropical cyclone, Ph.D. dissertation, Dep. of Atmos. Sci., Univ. of Illinois, Urbana, IL, 2008.
Zhang, H., McFarquhar, G. M., Saleeby, S. M., and Cotton, W. R.: Impacts of Saharan dust as CCN on the evolution of an idealized tropical cyclone, Geophys. Res. Lett., 34, L14812, doi:10.1029/2007GL029876, 2007.
Zhang, H., McFarquhar, G. M., Cotton, W. R., and Deng, Y.: Direct and indirect impacts of Saharan dust acting as cloud condensation nuclei on tropical cyclone eyewall development, Geophys. Res. Lett., 36, L06802, doi:10.1029/2009GL037276, 2009.
Zipser, E. J., Twohy, C. H., Tsay, S. C., Thornhill, K. L., Tanelli, S., Ross, R., Krishnamurti, T. N., Ji, Q., Jenkins, G., Ismail, S., Hsu, N. C., Hood, R., Heymsfield, G. M., Heymsfield, A., Halverson, J., Goodman, H. M., Ferrare, R., Dunion, J. P., Douglas, M., Cifelli, R., Chen, G., Browell, E. V., and Anderson, B.: The Saharan Air Layer and the fate of African Easterly Waves – NASA's AMMA field study of tropical cyclogenesis, B. Am. Meteorol. Soc., 90, 1137–1156, 2009.

ACPD
11, 14339–14381, 2011

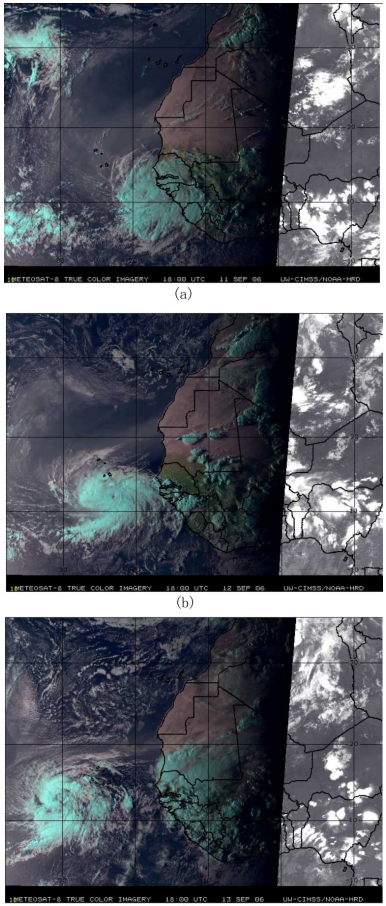

Fig. 1. Meteosat-8 visible imageries at 18:00 UTC on **(a)** 11, **(b)** 12 and **(c)** 13 September.

ACPD
11, 14339–14381, 2011

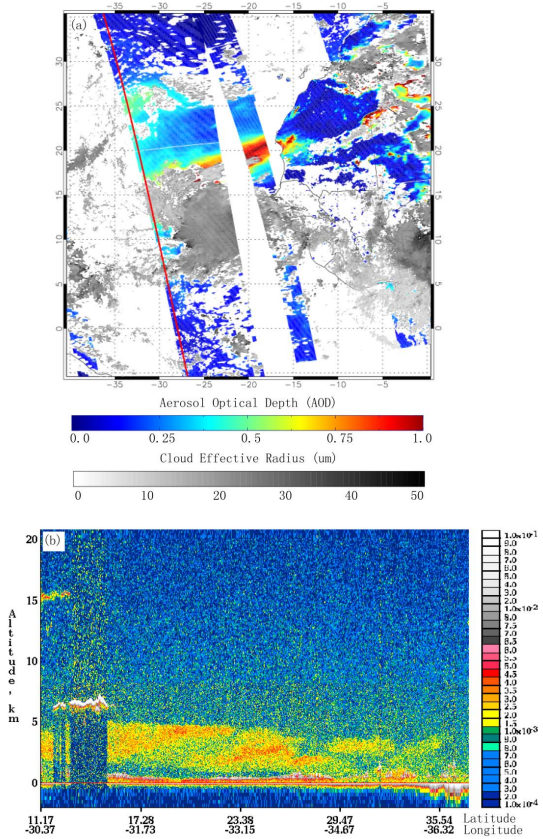

Fig. 2. **(a)** MODIS Aqua AOD and cloud effective radius (μm) between 13:55 UTC and 15:40 UTC 12 September. Red line indicated the path of CALIPSO. **(b)** Vertical profile of CALIPSO total attenuated back scatter ($km^{-1}\,sr^{-1}$) taken between 15:38 and 15:44 UTC on 12 September (image courtesy of http://www-calipso.larc.nasa.gov).

ACPD
11, 14339–14381, 2011

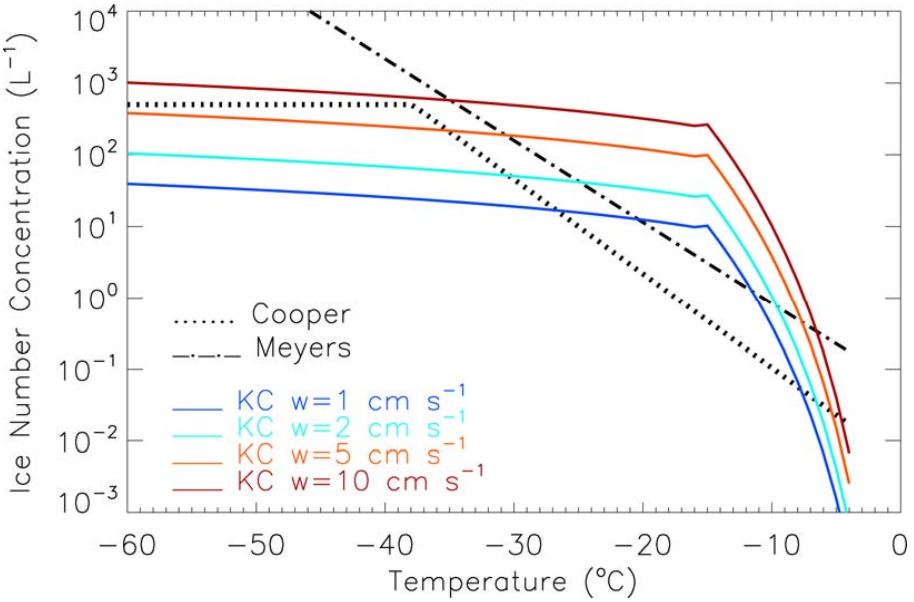

Fig. 3. Ice number concentration as a function of temperature for Meyers et al. (1992), Cooper (1986), and KC scheme. Four representative vertical velocities (w) of 1, 2, 5, and 10 cm s^{-1} are chosen to demonstrate the sensitivity of KC scheme to w. Meyers scheme is in the form of $N = \exp[-2.8 + 0.262(273.15 - T)]$ and Cooper scheme is given by $N = 0.005 \times \exp[0.304(273.15 - T)]$ with the maximum constrained at 500 l^{-1}.

ACPD
11, 14339–14381, 2011

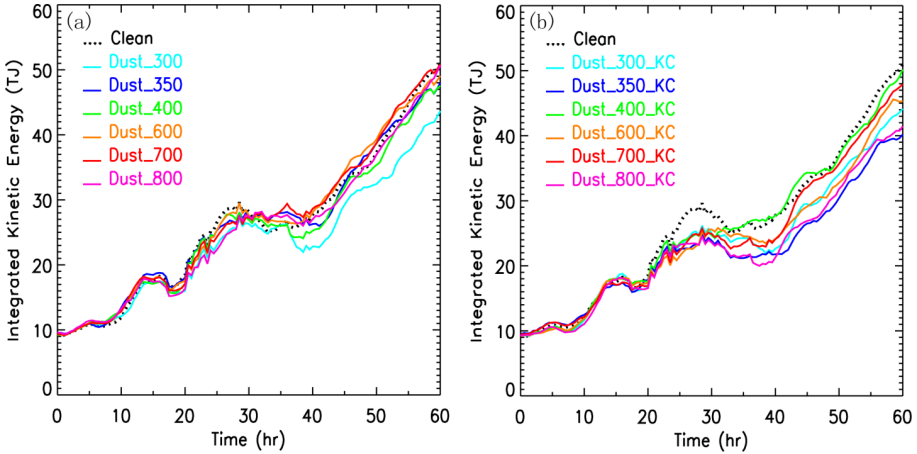

Fig. 4. Integrated Kinetic Energy (IKE) of the Clean (dotted line) and dust simulations (solid lines) with **(a)** the original Morrison scheme and **(b)** Morrison scheme with the KC ice parameterization.

ACPD
11, 14339–14381, 2011

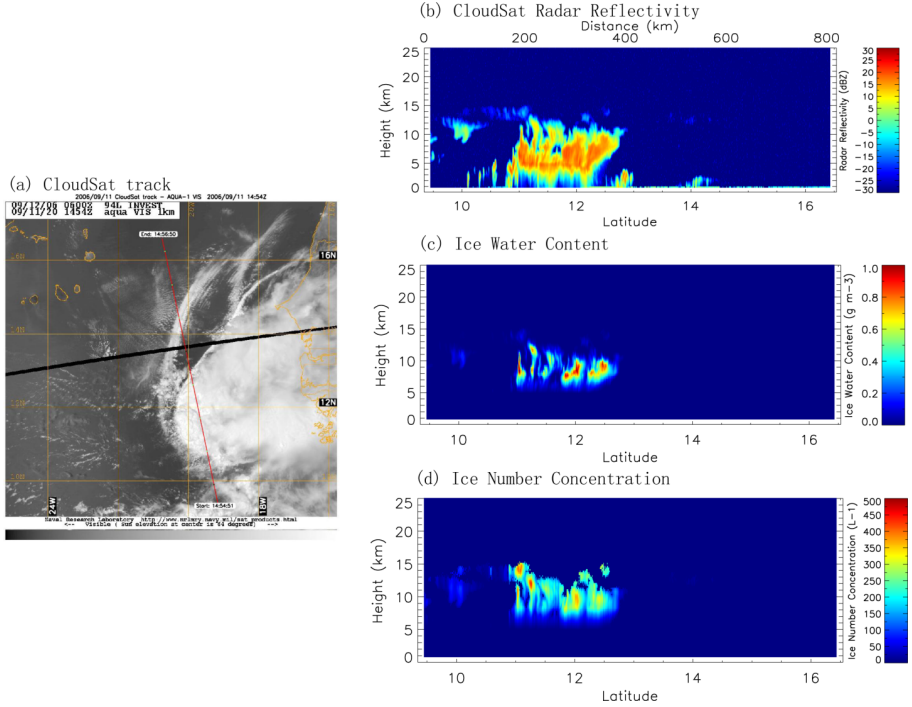

Fig. 5. **(a)** CloudSat path from 14:54 UTC to 14:56 UTC 11 September overlaid on visible satellite image from MODIS Aqua. **(b)** CloudSat retrieved radar reflectivity, **(c)** IWC, and **(d)** ice number concentration.

ACPD
11, 14339–14381, 2011

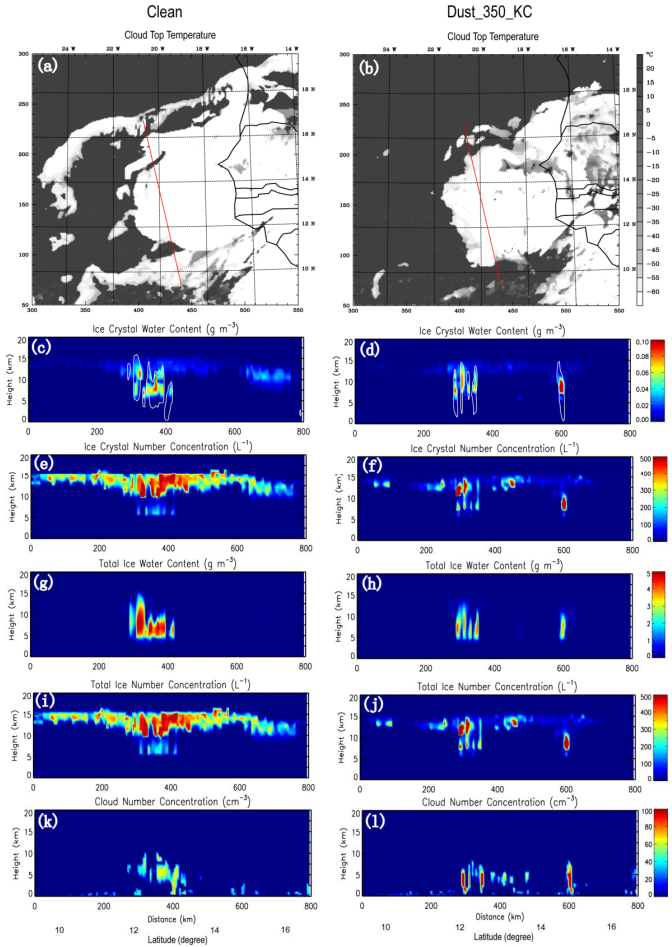

Fig. 6. Simulated ice and cloud properties along the CloudSat track for Clean at 03:00 UTC 12 September (left panels) and Dust_350_KC at 04:00 UTC 12 September (right panels) when the storms moved to a similar geolocation as observed by the CloudSat. The cross section follows the CloudSat track from south to north and is illustrated by the red line overlaid on the simulated cloud temperature **(a)** and **(b)**. The white solid line in **(a)** and **(b)** shows the contour of 1 m s^{-1} updraft.

ACPD
11, 14339–14381, 2011

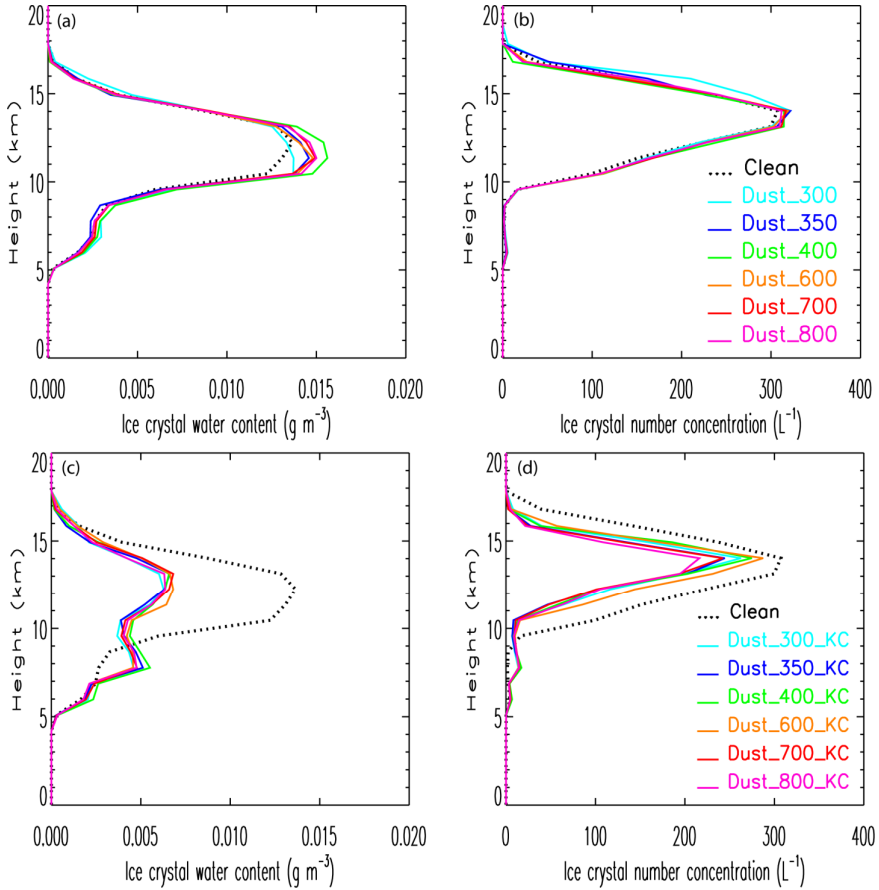

Fig. 7. Averaged ice crystal water content and number concentration over the entire storm area for simulations with the original Morrison scheme (top panels) and KC scheme (bottom panels) at the time when the CloudSat comparison was made (Fig. 6).

ACPD
11, 14339–14381, 2011

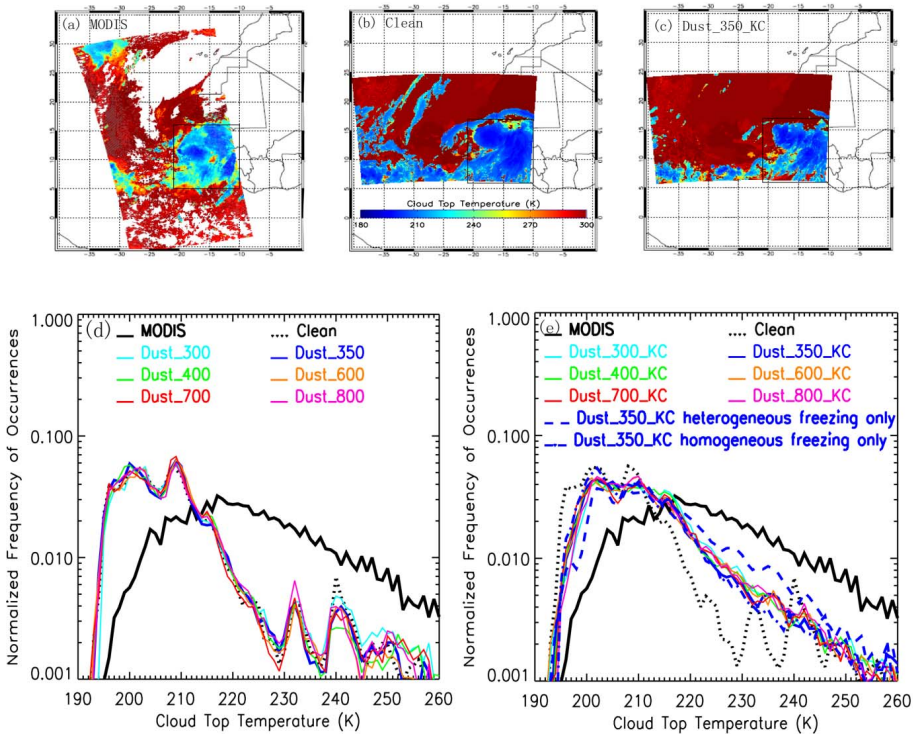

Fig. 8. **(a)** Cloud top temperature retrieved by MODIS between 14:50 UTC and 14:55 UTC 11 September; **(b)** Cloud top temperature derived from Clean at 23:00 UTC 11 September when the simulated storm moved to a similar location as the observed one; **(c)** The same as **(b)** except for Dust_350_KC; **(d)** Normalized frequency of occurrences for the MODIS retrieved and simulated cloud top temperature for simulations with the original Morrison scheme using data within the rectangular boxes shown on **(a)** and **(b)**; and **(e)** the same as **(d)** except for simulations with the KC scheme.

ACPD
11, 14339–14381, 2011

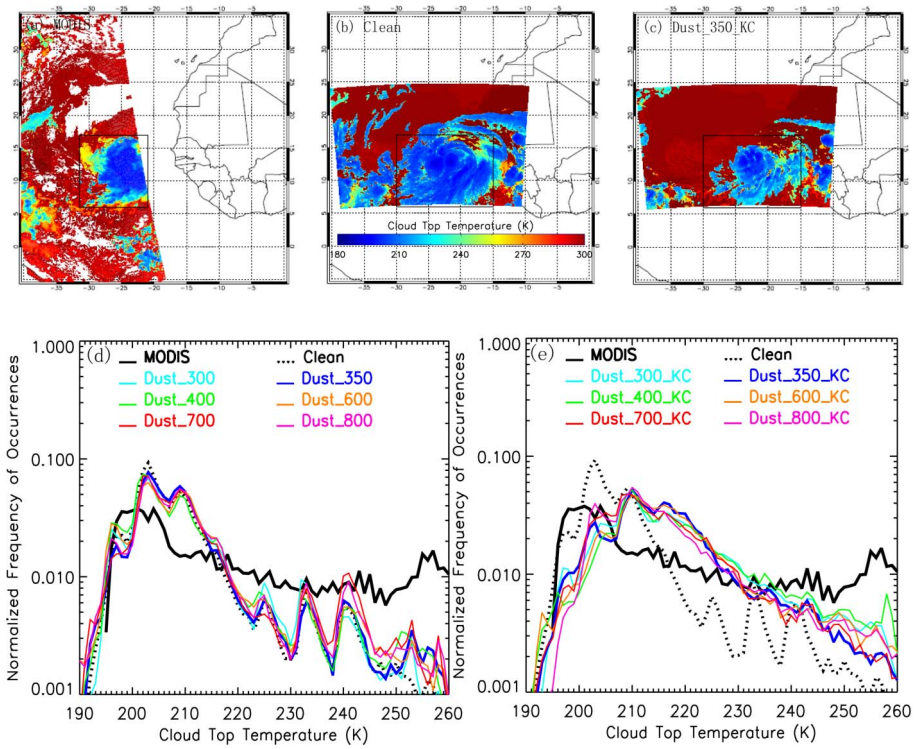

Fig. 9. The same as Fig. 8 except for using the data from the MODIS retrieval between 15:30 UTC and 15:40 UTC 12 September and cloud top temperature from simulations at 23:00 UTC 12 September.

ACPD
11, 14339–14381, 2011

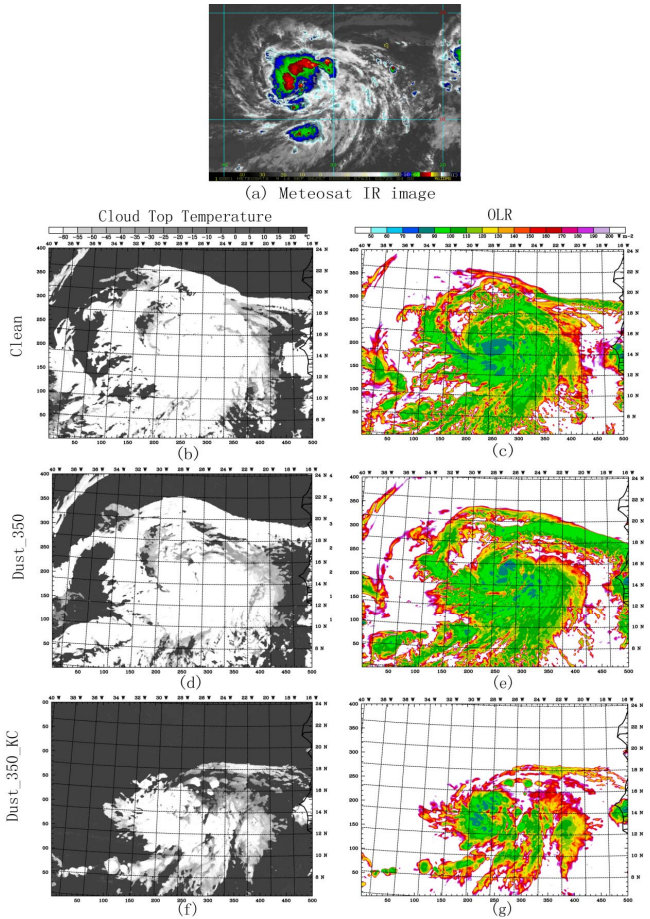

Fig. 10. (a) Meteosat IR imagery at 00:00 UTC 14 September (courtesy of Dr. John Knaff from the NOAA/NESDIS). Cloud top temperature (left panels) and OLR (right panels) distributions at the same time are shown for the Clean, Dust_350, and Dust_350_KC.

ACPD
11, 14339–14381, 2011

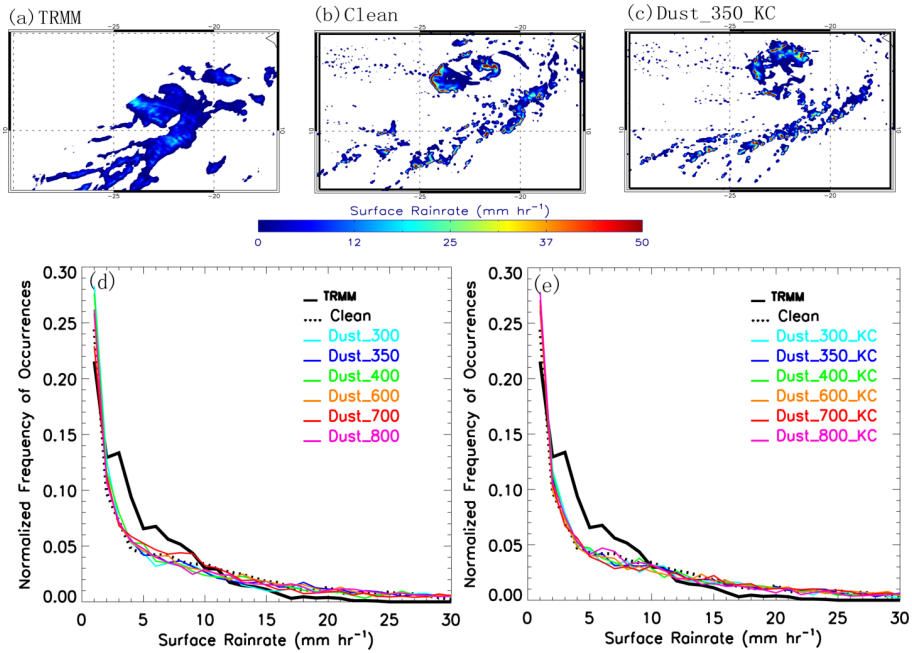

Fig. 11. **(a)** TRMM TMI surface rainrate at 14:06 UTC 12 September; **(b)** Surface rainrate from Clean at 23:00 UTC 12 September; **(c)** Surface rainrate from Dust_350 at 23:00 UTC 12 September; **(d)** Normalized frequency of occurrences of the TRMM TMI and simulated surface rainrate from simulations with the original Morrison scheme; and **(e)** the same as **(d)** except for simulations with the KC scheme.

ACPD
11, 14339–14381, 2011

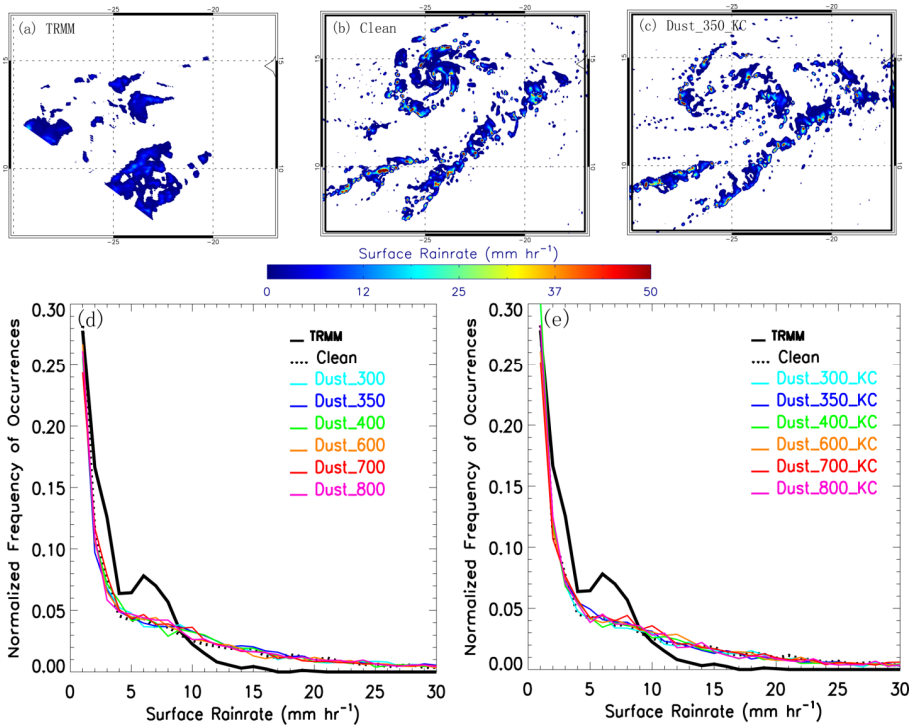

Fig. 12. The same as Fig. 11 except for using the data from TRMM TMI surface rainrate at 23:59 UTC 12 September and model output from 12:00 UTC 13 September.

ACPD
11, 14339–14381, 2011

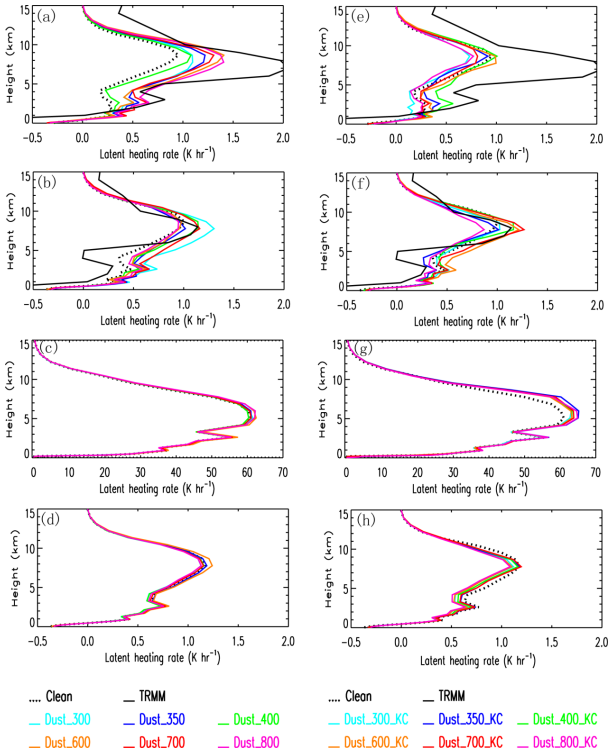

Fig. 13. Vertical profiles of the latent heating rate from simulations with the original Morrison scheme (left panels) and the KC scheme (right panels) at 23:00 UTC 12 September (first row), at 12:00 UTC 13 September (second row), over the entire 60 h period for region with vertical velocity greater than 1 m s^{-1} (third row) and over the entire 60 h period (fourth row). The latent heating profile was calculated by averaging within an area of 750 km by 750 km covering the storm main area. Latent heating profiles retrieved from TRMM TMI at 14:06 UTC 12 September are plotted on **(a)** and **(e)** when simulated storms moved to similar geolocation as shown in Fig. 11. TMI-retrieved heating profiles at 23:59 UTC 12 September are overlaid on **(b)** and **(f)** when simulated storms reached similar geolocation as shown in Fig. 12.

ACPD
11, 14339–14381, 2011

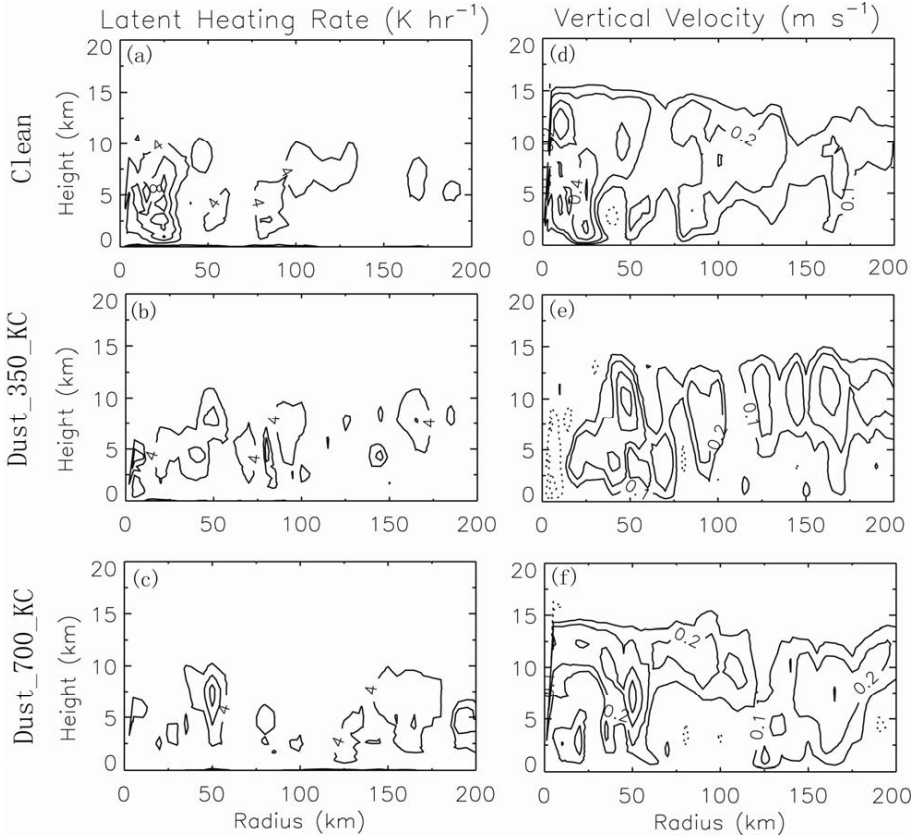

Fig. 14. Azimuthally averaged latent heating rate (left panels) and vertical velocity (right panels) for the Clean, Dust_350_KC, and Dust_700_KC simulation at 00:00 UTC 14 September.

ACPD
11, 14339–14381, 2011